Int. J. Appl. Math. Comput. Sci., 2002, Vol.12, No.2, 221–233

FUZZY AND NEURAL CONTROL OF AN INDUCTION MOTOR

MOULOUD AZZEDINE DENAI*, SID AHMED ATTIA*

* University of Science and Technology of Oran, Faculty of Electrical Engineering
B.P. 1505 El Mnaouar, Oran 31 000, Algeria
e-mail: denai@mail.univ-usto.dz, Ahmed.Attia@lag.ensieg.inpg.fr

This paper presents some design approaches to hybrid control systems combining conventional control techniques with fuzzy logic and neural networks. Such a mixed implementation leads to a more effective control design with improved system performance and robustness. While conventional control allows different design objectives such as steady state and transient characteristics of the closed loop system to be specified, fuzzy logic and neural networks are integrated to overcome the problems with uncertainties in the plant parameters and structure encountered in the classical model-based design. Induction motors are characterised by complex, highly non-linear and time-varying dynamics and inaccessibility of some states and outputs for measurements, and hence can be considered as a challenging engineering problem. The advent of vector control techniques has partially solved induction motor control problems, because they are sensitive to drive parameter variations and performance may deteriorate if conventional controllers are used. Fuzzy logic and neural network-based controllers are considered as potential candidates for such an application. Three control approaches are developed and applied to adjust the speed of the drive system. The first control design combines the variable structure theory with the fuzzy logic concept. In the second approach neural networks are used in an internal model control structure. Finally, a fuzzy state feedback controller is developed based on the pole placement technique. A simulation study of these methods is presented. The effectiveness of these controllers is demonstrated for different operating conditions of the drive system.

Keywords: fuzzy control, neural networks, induction motor, vector control, speed observer

1. Introduction

AC motors, particularly the squirrel-cage induction motor (SCIM), enjoy several inherent advantages like simplicity, reliability, low cost and virtually maintenance-free electrical drives. However, for high dynamic performance industrial applications, their control remains a challenging problem because they exhibit significant non-linearities and many of the parameters, mainly the rotor resistance, vary with the operating conditions. Field orientation control (FOC) or vector control (Vas, 1990) of an induction machine achieves decoupled torque and flux dynamics leading to independent control of the torque and flux as for a separately excited DC motor. FOC methods are attractive but suffer from one major disadvantage: they are sensitive to motor parameter variations such as the rotor time constant and an incorrect flux measurement or estimation at low speeds (Trzynadlowski, 1994). Consequently, performance deteriorates and a conventional controller such as a PID is unable to maintain satisfactory performance under these conditions.

Recently, there has been observed an increasing interest in combining artificial intelligent control tools with classical control techniques. The principal motivations for such a hybrid implementation is that with fuzzy logic and neural networks issues such as uncertainty or unknown variations in plant parameters and structure can be dealt with more effectively, hence improving the robustness of the control system. Conventional controls have on their side well-established theoretical backgrounds on stability and allow different design objectives such as steady state and transient characteristics of the closed loop system to be specified. Several works contributed to the design of such hybrid control schemes (Cao *et al.*, 1996; Chen and Chang, 1998; Shaw and Doyle, 1997).

In this paper three control methods are introduced and applied to an indirect field-oriented induction motor. In the first design approach the basic fuzzy logic controller (FLC), regarded as a kind of variable structure controller (VSC) (Hung *et al.*, 1993) for which stability and robustness are well established, is developed. This follows the interpretation of linguistic IF–THEN rules as a set of controller structures that are switched according to the process states (Kawaji and Matsunaga, 1994).

The second design approach is based on the well-known internal model control concept (Morari and Zafiriou, 1989). To improve the robustness of the controller, neural networks are introduced to form the forward and inverse model control algorithm in place of the classical model-based structure. In the third approach, the ba-

sic idea of the proposed controller is similar to the gain-scheduling technique. The design is based on a reduced-order state space model of the motor drive from which a family of local state space models covering the operating range of the drive system are defined. We then use the state feedback design concept to get a linear state feedback controller for each local model (Cao *et al.*, 1999; Mei *et al.*, 1998). These local controllers are inferred into one global state feedback controller using a simple fuzzy inference technique.

These controllers are evaluated under simulations for a variety of operating conditions of the drive system and the results demonstrate the ability of the proposed control structures to improve the performance and robustness of the drive system. A speed observer based on neural networks is designed and included in the closed-loop control structure to achieve a sensorless operation of the drive system.

2. Induction Motor Equations

The d-q dynamic model of the SCIM with the reference frame fixed to the stator is given by (Trzynadlowski, 1994)

$$\frac{\mathrm{d}}{\mathrm{d}t}\begin{bmatrix} i_{ds}^s \\ i_{qs}^s \\ i_{dr}^s \\ i_{qr}^s \end{bmatrix} = \frac{1}{L_\sigma^2}\left(\begin{bmatrix} L_r & 0 & -L_m & 0 \\ 0 & L_r & 0 & -L_m \\ -L_m & 0 & L_s & 0 \\ 0 & -L_m & 0 & L_s \end{bmatrix} \begin{bmatrix} V_{ds}^s \\ V_{qs}^s \\ 0 \\ 0 \end{bmatrix} + \begin{bmatrix} -R_s L_r & \omega L_m^2 & R_r L_m & \omega L_r L_m \\ -\omega L_m^2 & -R_s L_r & -\omega L_r L_m & R_r L_m \\ R_s L_m & -\omega L_s L_m & -R_r L_s & -\omega L_s L_m \\ \omega L_s L_m & R_s L_m & \omega L_s L_m & -R_r L_s \end{bmatrix} \begin{bmatrix} i_{ds}^s \\ i_{qs}^s \\ i_{dr}^s \\ i_{qr}^s \end{bmatrix} \right), \quad (1)$$

where

$$L_\sigma = \sqrt{L_s L_r - L_m^2}.$$

The electromagnetic torque is found as

$$T_e = \frac{2pL_m}{3L_r}\left(i_{qs}^s \Phi_{dr}^s - i_{dr}^s \Phi_{qr}^s\right), \quad (2)$$

where

$$\Phi_{ds}^s = L_r i_{dr}^s + L_m i_{ds}^s, \quad \Phi_{qs}^s = L_r i_{qr}^s + L_m i_{qs}^s \quad (3)$$

are the rotor flux components expressed in the stator reference frame.

The field orientation principle is based on the following conditions which are expressed in the excitation reference frame:

$$\Phi_{qr}^e = 0, \quad \Phi_{dr}^e = \text{constant}. \quad (4)$$

Hence the equations ensuring the field orientation are expressed as

$$i_{ds}^{e^*} = \frac{1 + T_r s}{L_m}\Phi_{dr}^{e*}, \quad i_{ds}^{e^*} = \frac{T_e^*}{K_T \Phi_{dr}^{e^*}}, \quad (5)$$

where $T_r = L_r/R_r$ is the rotor time constant.

Under these conditions, the induction machine is transformed into a linear current/torque converter:

$$T_e = K_T \Phi_{dr}^e i_{qs}^e. \quad (6)$$

Hence the rotor torque and flux may be controlled separately through i_{qs} and i_{ds}, respectively. The adequate torque reference T_e^* is generated from the speed error via the controller while the flux reference Φ_r^* is kept constant for each operating point.

In order to design a controller, the reduced-order model of the SCIM given by Fig. 1 is used. Here T_L

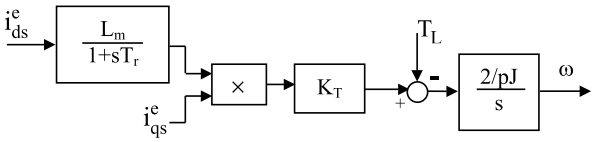

Fig. 1. Simplified field-oriented model of the SCIM.

is the disturbance torque. The state space representation is obtained as

$$\begin{bmatrix} \dot{x}_1 \\ \dot{x}_2 \end{bmatrix} = \begin{bmatrix} 0 & 1 \\ 0 & -T_r^{-1} \end{bmatrix} \begin{bmatrix} x_1 \\ x_2 \end{bmatrix} + \begin{bmatrix} 0 \\ K_T'/T_r \end{bmatrix} i_{qs}^e, \quad (7)$$

where $x_1 = \omega$, $x_2 = \mathrm{d}\omega/\mathrm{d}t$ and

$$K_T = \frac{3pL_m}{4L_r}, \quad K_T' = \frac{2}{pJ} L_m K_T i_{ds}^e. \quad (8)$$

3. Speed Controller Design

The overall block diagram of a current controlled PWM induction motor with indirect field orientation is given in Fig. 2. The field-oriented control block receives the computed torque from the speed controller and the flux from the field weakening block. In the look-up table used for field-weakening, the flux is assumed to be constant when the motor operates below the rated speed, and beyond the rated speed the flux speed product is held constant.

The FOC block performs the slip calculation and generates $i_{qs}^{e^*}$ and $i_{ds}^{e^*}$. Inside the qde to the abc transformation block, the following transformations are performed:

$$qde \rightarrow qds \begin{cases} i_{qs}^{s^*} = i_{qs}^{e^*}\cos\theta_s + i_{ds}^{e^*}\sin\theta_s, \\ i_{ds}^{s^*} = -i_{qs}^{e^*}\sin\theta_s + i_{ds}^{e^*}\cos\theta_s, \end{cases} \quad (9)$$

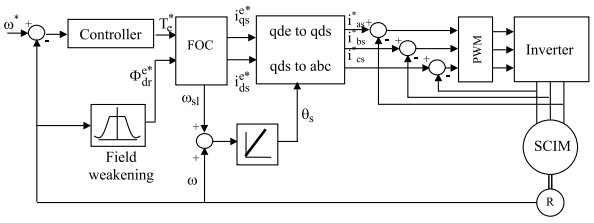

Fig. 2. Speed control of the current regulated indirect field-oriented induction motor.

$$qds \rightarrow abc \begin{cases} i_{as}^* = i_{qs}^{s^*}, \\ i_{bs}^* = -\dfrac{1}{2} i_{qs}^{s^*} - \dfrac{\sqrt{3}}{2} i_{ds}^{s^*}, \\ i_{cs}^* = -\dfrac{1}{2} i_{qs}^{s^*} + \dfrac{\sqrt{3}}{2} i_{ds}^{s^*}. \end{cases} \tag{10}$$

Here θ_s represents the sum of the slip and rotor angles.

A sinusoidal current source of variable magnitude and frequency is used to represent the fundamental component of the actual PWM inverter waveform. This avoids lengthy simulation times caused by the PWM switchings. Nevertheless, such a simulation study can still provide some understanding of the control strategies implementation, tuning and analysis.

3.1. Fuzzy Variable Structure Control (FVSC)

The VSC strategy consists in switching to a different control structure on each side of a given switching surface according to a predefined switching function. An interesting characteristic of the VSC is that under certain conditions the system responds with a sliding mode on the switching surface and in this mode the system is insensitive to parameter variations and disturbances.

The basic control law of Variable Structure Systems (VSS) is given by

$$u = -K \operatorname{sgn}(S), \tag{11}$$

where K is a constant parameter, $\operatorname{sgn}(\cdot)$ is the sign function and S is the switching function defined by

$$S = f^T x. \tag{12}$$

When $S = 0$, this represents the switching surface and gives the desired dynamics.

Similarly, the fuzzy rules

$$R_i: \text{ IF } A_i \text{ AND } B_i \text{ THEN } C_i \tag{13}$$

may be interpreted as a control structure that is switched according to the system states. Hence fuzzy controllers can be viewed as a class of variable structure controllers.

Let the desired dynamics of the drive system be specified in terms of the switching surface shown in Fig. 3. The error trajectory approaches the switching surface gradually with the slopes $-m_f$ and $-m_s$ corresponding to fast and slow dynamics, respectively.

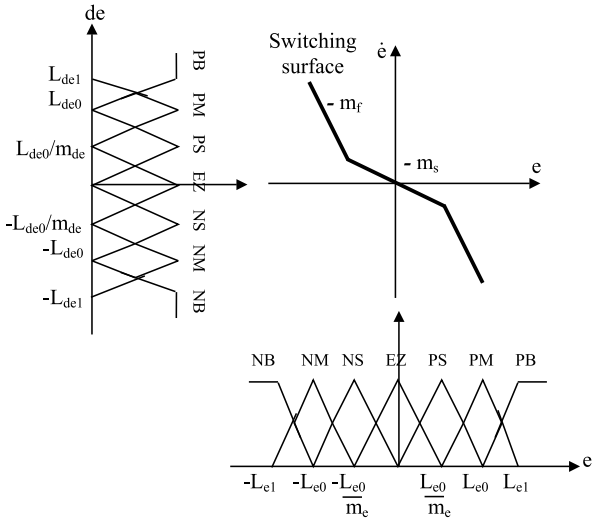

Fig. 3. Membership functions adjustment with m_s and m_f.

With reference to Fig. 3, the slopes of the error trajectory are obtained as

$$m_s = \frac{L_{de0} m_e}{L_{e0} m_{de}},$$
$$m_f = \frac{L_{de0} - \dfrac{L_{de0}}{m_{de}}}{L_{e0} - \dfrac{L_{e0}}{m_e}} = \frac{L_{de1} - \dfrac{L_{de1}}{m_{de}}}{L_{e1} - \dfrac{L_{e1}}{m_e}}. \tag{14}$$

By specifying the desired m_s and m_f, and assuming the range of the error signal $\{L_e,\ m_e\}$, the membership functions related to the error and its change of triangular shape chosen here are adjusted by the following relationships:

$$m_{de} = \frac{L_{de0} m_e}{m_s L_{e0}},$$
$$L_{dei} = m_f L_{ei} - (m_f - m_s)\frac{L_{e0}}{m_e}, \quad i = 0, 1. \tag{15}$$

The controller structure is Proportional-Integral (PI) and is illustrated in Fig. 4.

Here $K_P = K_u R(K_{de})$ and $K_I = K_u R(K_e)$ are the controller proportional and integral gains, and $R(\cdot)$ is defined by the controller rule base which is summarized in Table 1. Here NB (Negative Big), NM (Negative Medium), NS (Negative Small), Z (Zero), PS (Positive Small), PM (Positive Medium) and PB (Positive Big)

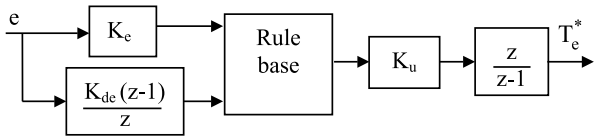

Fig. 4. Fuzzy PI controller structure.

are linguistic variables. The max-min inference method was used and the defuzzification procedure was based on the centre of area method.

Table 1. FVSC rule.

		← e →						
		NB	**NM**	**NS**	**EZ**	**PS**	**PM**	**PB**
	PB	**Z**	PS	PM	PB	PB	PB	PB
↑	**PM**	NS	**Z**	PS	PM	PB	PB	PB
	PS	NM	NS	**Z**	PS	PM	PB	PB
de	**EZ**	NB	NM	NS	**Z**	PS	PM	PB
	NS	NB	NB	NM	NS	**Z**	PS	PM
↓	**NM**	NB	NB	NB	NM	NS	**Z**	PS
	NB	NB	NB	NB	NB	NM	NS	**Z**

3.2. Internal Model Controller Based on Neural Networks (NIMC)

The basic architecture of a classical internal model controller (IMC) is illustrated in Fig. 5 (Morari and Zafiriou, 1989). A system model G_m is placed in parallel with the actual system G. The control signal u is applied simultaneously to the system and the system model. The difference $y-y_m$, which gives an estimate of the disturbance d and/or system changes, is used to adjust the command signal y^*. An attractive feature of the IMC is that it produces an offset-free response even when the system is subjected to a constant disturbance.

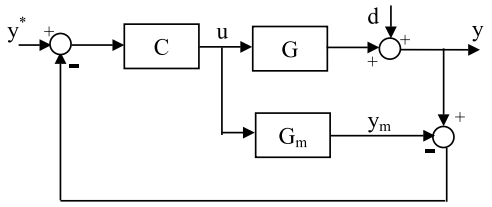

Fig. 5. IMC structure.

If a perfect model is assumed $(G = G_m)$, then the closed-loop system is stable if the controller C and the system are stable. However, under mismatch conditions $(G \neq G_m)$, a low pass filter is introduced in the feedback loop to improve the controller robustness with respect to modelling errors.

Since the controller is the inverse of the system model (i.e. $C = G_m^{-1}$), the system model should be inverse stable. Although this design technique produces a robust controller, it does require a model of the controlled process to be formulated and hence it possesses the shortcomings of model-based control techniques.

Artificial Neural Networks (ANN's) are potential candidates for approximating complex non-linear process dynamics and have been used to formulate a variety of control strategies (Hunt and Sbarbaro, 1991; Hunt *et al.*, 1992; Kwan and Lewis, 2000). There are two basic design approaches:

- Direct design, where the neural network is itself the controller. The most fundamental method is termed *direct inverse control*. It uses a trained inverse model of the process as a controller.
- Indirect design: the controller uses a neural network to predict the process output.

In the following, ANN's are used in combination with an IMC structure to give the overall SCIM control system depicted in Fig. 6. Here Net 1 and Net 2 are neural networks

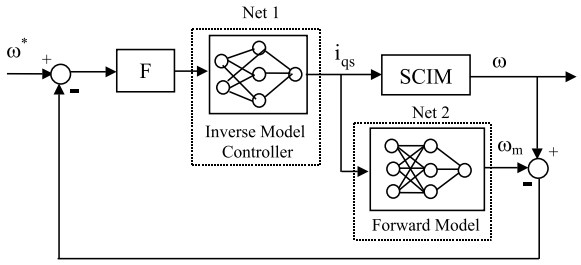

Fig. 6. Neural network-based IMC control.

representing the SCIM inverse and forward models, respectively. F is a first-order compensating filter included to provide the desirable transient response and robustness chosen as

$$F(z) = \frac{1-\alpha}{z-\alpha}, \quad 0 < \alpha < 1. \tag{16}$$

With reference to Fig. 1, the speed transfer function is obtained as

$$\omega = \frac{2}{p}\frac{\Phi_r i_{qs} K_T}{sJ} = \frac{K'_T}{s} i_{qs}. \tag{17}$$

Discretizing (17) with a sampling period T_s leads to the following difference equation:

$$\omega(k) = \omega(k-1) + K''_T\big[i_{qs}(k) + i_{qs}(k-1)\big], \tag{18}$$

where

$$K''_T = K'_T \frac{T_s}{2}. \tag{19}$$

The SCIM neural network model Net 2 is a Multilayer Perceptron (MLP) with a three-neuron input layer, a ten-neuron hidden layer and a one-neuron output layer trained using the Levenberg-Marquardt Algorithm (LMA) (Si and Zhou, 1996) as illustrated in Fig. 7(a).

The inverse model is described by the following difference equation:

$$i_{qs}(k) = \frac{1}{K_T''}\big[\omega(k) - \omega(k-1)\big] - i_{qs}(k-1). \quad (20)$$

The stability of the training process is improved by using a different discretisation procedure. For small T_s the difference equation is obtained as

$$(z-1)\omega(k) = 2K_T'' i_{qs}(k). \quad (21)$$

The inverse model is trained with the same procedure as illustrated in Fig. 7(b).

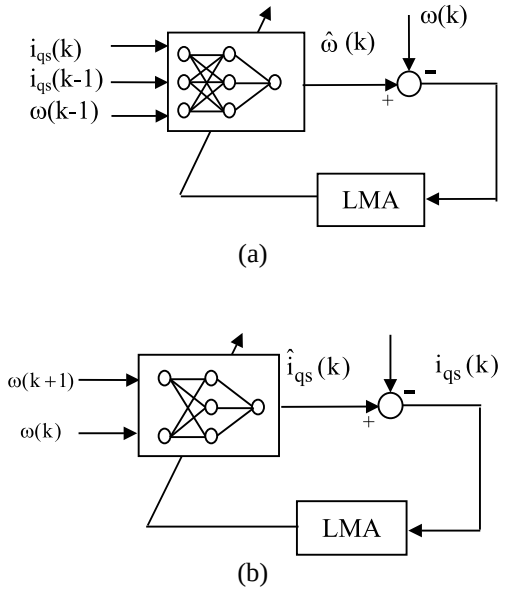

Fig. 7. Training of the forward (a) and the inverse (b) SCIM neural model based on the reduced-order model.

Finally, a reference model is introduced to overcome the problem associated with the future value $\omega(k+1)$. The overall block diagram of the closed-loop control system is represented in Fig. 8.

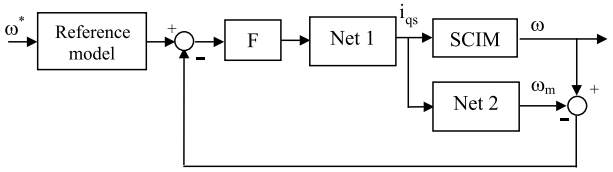

Fig. 8. Closed-loop system structure.

3.3. Fuzzy State Feedback Controller (FSFC)

To formulate the design problem, assume that a family of linear state space models can be obtained for different operating points of the system. A related global fuzzy model can be formulated by the following rules (Cao *et al.*, 1999):

$$R^i:\ \text{IF } x_1 \text{ is } F_1^i \text{ AND } x_2 \text{ is } F_2^i \ldots \text{ AND } x_n \text{ is } F_n^i,$$
$$\text{THEN } \begin{cases} \dot{x} = A_i x + B_i u, \\ y = Cx, \end{cases} \quad i = 1, \ldots, L. \quad (22)$$

The nominal model can be described analytically by

$$\dot{x} = A_0 x + B_0 u \quad (23)$$

with

$$A_0 = \sum_{i=1}^{L} \mu_i A_i, \quad B_0 = \sum_{i=1}^{L} \mu_i B_i, \quad (24)$$

μ_i being the membership factor for the i-th rule using the sum-prod inference method.

The basic idea is to develop for each rule a state feedback control law using the classical pole placement topology. These local controllers are inferred into one global fuzzy state feedback controller for the overall operating regimes of the system.

The state feedback is formulated as

$$R^i:\ \text{IF } x_1 \text{ is } F_1^i \text{ AND } x_2 \text{ is } F_2^i \ldots \text{ AND } x_n \text{ is } F_n^i,$$
$$\text{THEN } \begin{cases} \dot{x} = A_i x + B_i u, \\ u = -K_i x, \end{cases} \quad i = 1, \ldots, L, \quad (25)$$

where K_i is the gain vector related to the $(A_i,\ B_i)$ state space model computed using Ackermann's algorithm.

These local state feedback controllers are inferred into one global fuzzy state feedback controller for the overall operating regimes of the drive system:

$$K = \sum_{i=1}^{L} \mu_i K_i. \quad (26)$$

Hence the fuzzy rules related to the motor speed are formulated as follows:

$$R^i:\ \text{IF } x_1 \text{ is } F^i,$$
$$\text{THEN } \begin{bmatrix} \dot{x}_1 \\ \dot{x}_2 \end{bmatrix} = \begin{bmatrix} 0 & 1 \\ 0 & -T_r^{-1} \end{bmatrix} \begin{bmatrix} x_1 \\ x_2 \end{bmatrix} + \begin{bmatrix} 0 \\ K_T'(F^i)/T_r \end{bmatrix} i_{qs}^e, \quad (27)$$

where F^i corresponds to the fuzzy set i defined by the linguistic labels {NG, NM, ... }, and $K'_T(F^i)$ is the gain value for a given interval.

Furthermore, an integral action was introduced in the control structure in order to cope with steady state errors. The overall control system configuration is shown in Fig. 9.

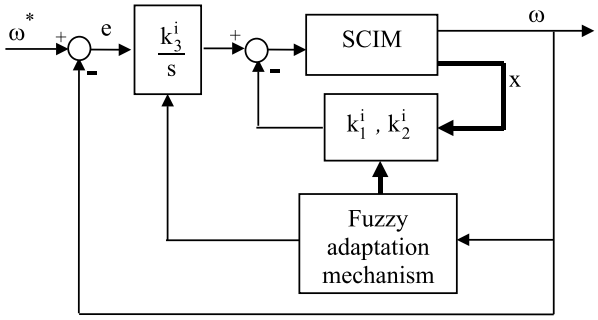

Fig. 9. Fuzzy state feedback configuration with integral action.

With reference to Fig. 9, the fuzzy adaptation mechanism is based on the following algorithm:

$$R^i: \text{ IF } x_1 \text{ is } F^i,$$

$$\text{THEN } \begin{bmatrix} \dot{x}_1 \\ \dot{x}_2 \end{bmatrix} = \begin{bmatrix} 0 & 1 \\ 0 & -T_r^{-1} \end{bmatrix} \begin{bmatrix} x_1 \\ x_2 \end{bmatrix} + \begin{bmatrix} 0 \\ K'_T(F^i)/T_r \end{bmatrix} i^e_{qs}, \tag{28}$$

$$i^e_{qs} = \frac{k^i_3}{s} e - k^i_1 x_1 - k^i_2 x_2, \tag{29}$$

where k^i_3 is the integral gain related to the operating point. The state feedback gain with integral action and the fuzzy controller gain are obtained as

$$K_i = \begin{bmatrix} k^i_1 & k^i_2 & k^i_3 \end{bmatrix}, \quad K = \sum_{i=1}^{5} \mu_i K_i. \tag{30}$$

4. Design of a Speed Observer

In the drive closed-loop control scheme a rotational transducer is often included to produce the speed measurement feedback signal. These sensors lower the system reliability in a hostile environment and increase the overall system investment. Recent investigations have been focused on the design of sensorless drives. Several approaches have been proposed (Elloumi *et al.*, 1998; Kim *et al.*, 1998; Tajima, 1993; Zhen and Xu, 1998). In what follows, a speed estimator is designed based on neural networks. In Appendix B the equations of a classical speed observer are derived.

Next, an MLP neural network with one ten-neuron hidden layer and logarithmic activation functions is applied to speed identification and trained according to the process described in Fig. 10.

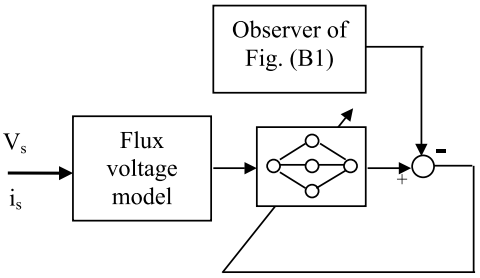

Fig. 10. Training of the neural network speed observer.

The neural network observer is trained to approximate the equation of the speed observer. In the training mode, a set of data was used to adjust interconnection weights of the network. Once these weights had been determined, the testing data (different from the training data) were fed to the network in order to evaluate the NN speed observer and to validate its generalisation capability. The training includes 5000 epochs and the testing includes 500 epochs.

The results are illustrated in Fig. 11, which demonstrates the ability of the trained neural network to track low- and high-speed waveforms. The neural network model was trained only under nominal speed conditions and the fluctuations observed at low-speed operation may be a result of this.

5. Performance Evaluation

The parameters of the induction motor considered in this study are summarised in Appendix A. The performances of the proposed controllers are evaluated separately under a variety of operating conditions.

5.1. FVSC

Initial simulations are performed in order to establish the suitable range of the design parameters m_f and m_s. In Fig. 12 the speed responses for different values of these parameters are shown. The tuning parameters were fixed to $[5\ 5]$, which produced satisfactory response characteristics in the simulations considered.

Next, the drive system under FVSC is subjected to a variable speed reference profile as illustrated in Fig. 13.

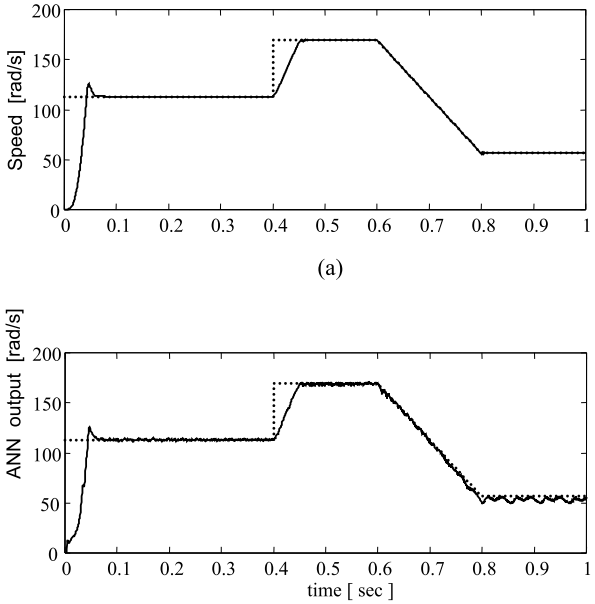

Fig. 11. Performance of the ANN-based speed observer for high- and low-speed conditions: (a) actual motor speed, (b) neural network output.

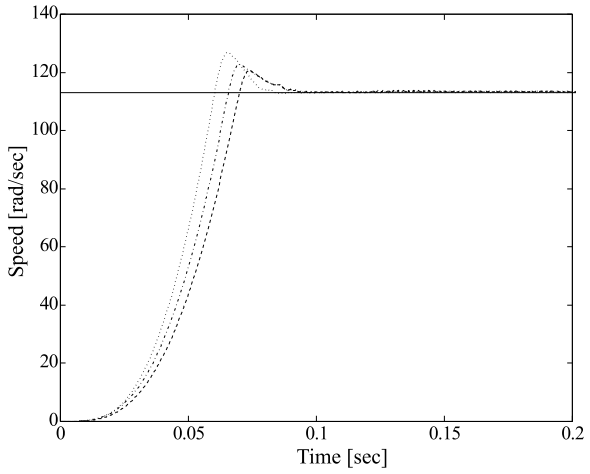

Fig. 12. Step response of the SCIM for different m_f and m_s: $[m_f\ m_s] = [10\ 5]$ (dotted), $[5\ 5]$ (dash-dot), $[5\ 10]$ (dashed).

As seen from the figure, the actual rotor speed overlaps the variable speed reference. The performance of the design controller is evaluated in the presence of load changes. In Fig. 14 the speed response under two load variations from 0 to 80 Nm and from 80 to 40 Nm applied at 0.6 sec and 0.8 sec, respectively, is shown. This result demonstrates the ability of the controller to produce the required torque compensating the component in order to maintain a stable response.

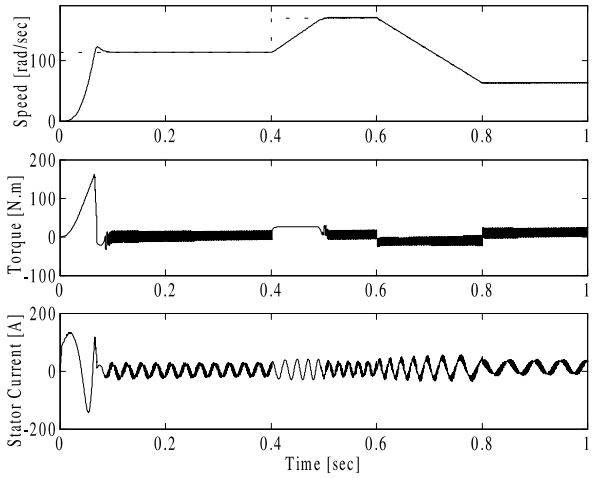

Fig. 13. Drive system response under a variable speed reference.

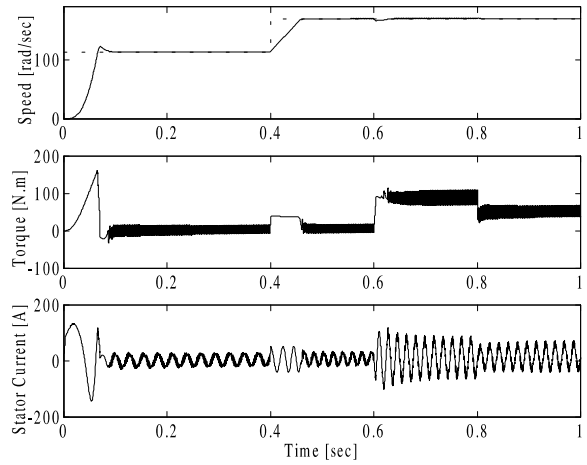

Fig. 14. Speed response with two load changes.

Speed sensorless operation of the drive system is illustrated in Fig. 15, which demonstrates comparable performance with extra small fluctuations in the response.

5.2. NIMC

The inverse and forward models Net1 and Net2 are based on the reduced-order model and applied to the actual SCIM model given by (1). Connecting Net2 in series with the SCIM model leads to a time shift between the input and output signals as illustrated by Fig. 16.

In IMC, the linear filter $F(z)$ is designed to provide a desirable robustness with respect to modelling errors and improves the tracking properties to the overall closed-loop drive system. In Fig. 17 the speed response is shown for different values of the filter cut-off frequency α. It appears that larger values of α slow down the response. In what follows, α is fixed to 0.5.

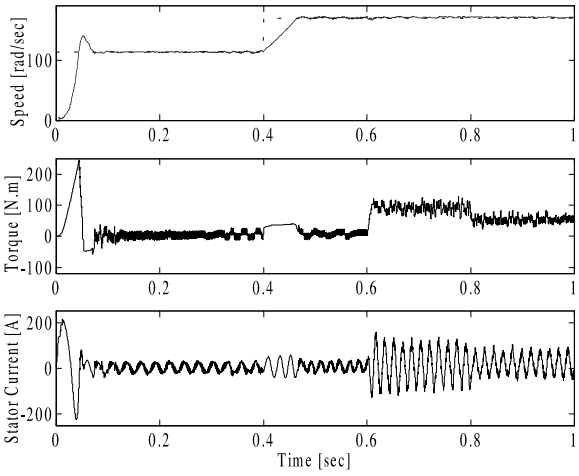

Fig. 15. Speed response with two load changes with neural network-based observer.

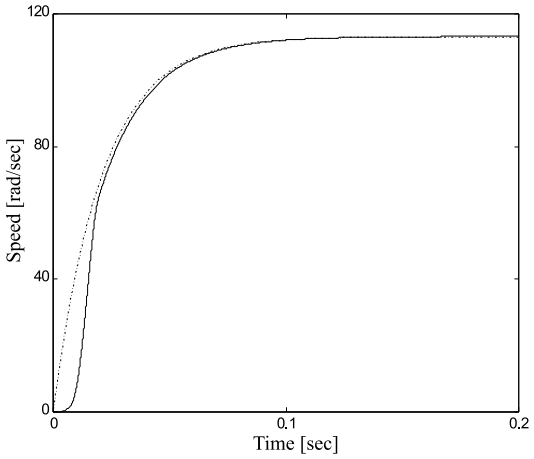

Fig. 16. Input and output signals of the series transfer function: input signal (first-order model, dashed), output signal (solid).

In the following simulation, the performance of the IMC structure based on a first-order reference model with a time constant of 0.021 sec is subjected to load changes. In Fig. 18, load variations are applied from 0 to 80 Nm and from 80 to 40 Nm at 0.6 sec and 0.8 sec, respectively.

The neural network model prediction error related to this result is given in Fig. 19. In the initial adaptation stage the neural network output exhibits some fluctuations due to the new operating conditions and this also affects the torque response. However, the controller is able to maintain a stable response, which confirms the robustness of the neural network-based IMC structure with respect to the model-based one.

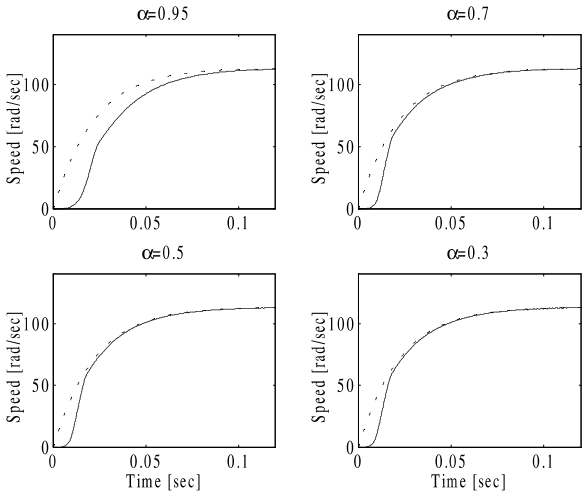

Fig. 17. Speed response for different values of α.

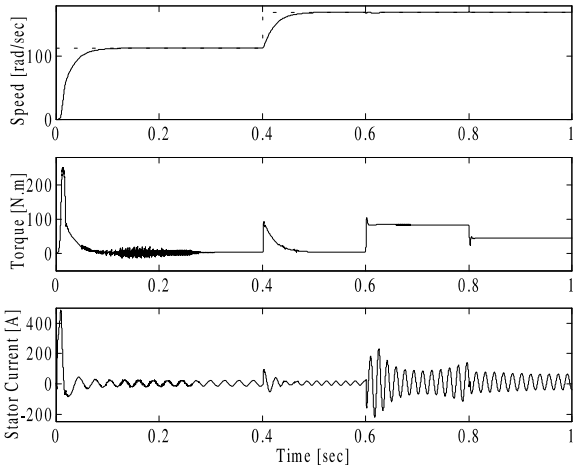

Fig. 18. NIMC speed control under load changes.

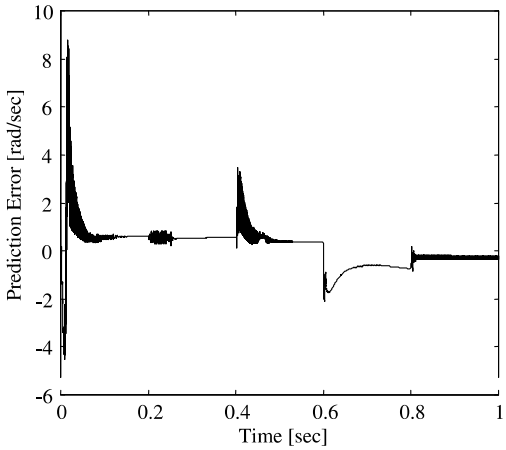

Fig. 19. Neural network model prediction error.

5.3. FSFC

In this simulation study five operating points are used for defining the fuzzy state space models using the reduced-order model of the induction motor corresponding to the speeds 1500, 1900, 2250, 2600 and 3000 rpm. On the basis of these local models, local state feedback controllers stabilizing the drive system around these operating points are designed using Ackerman's formula with the desired pole configurations shown in Table 2.

Table 2. Desired pole configurations for FSFC.

	Eigenvalue	Magnitude	Damping	Frequency
First	9.51e−1	9.51e−1	1.00	5.00e+1
pole confi-	9.44e−1+5.40e−2i	9.46e−1	7.00e−1	8.00e+1
guration	9.44e−1−5.40e−2i	9.46e−1	7.00e−1	8.00e+1
Second	9.79e−1 + 2.10e−2i	9.79e−1	7.00e−1	3.00e+1
pole confi-	9.79e−1−2.10e−2i	9.79e−1	7.00e−1	3.00e+1
guration	9.14e−1	9.14e−1	1.00	9.00e+1

Then the five controller gains are directly inferred into a global state feedback controller using a simple fuzzy inference procedure. The resulting membership function of the global controller is given in Fig. 20. The step responses related to the pole configurations given above are shown in Fig. 21.

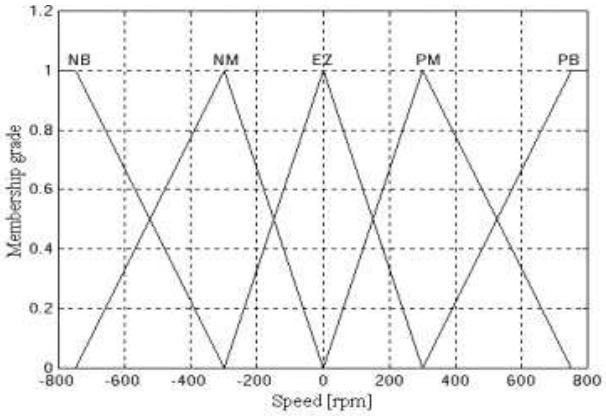

Fig. 20. FSFC membership function.

Next, the performance of FSFC with the first pole configuration is evaluated under different operating conditions of the drive system. The load torque is kept constant while the drive system is subjected to step changes and a slow ramp as shown by Fig. 22. The response to the ramp is rather slow, which can be improved by selecting different pole locations.

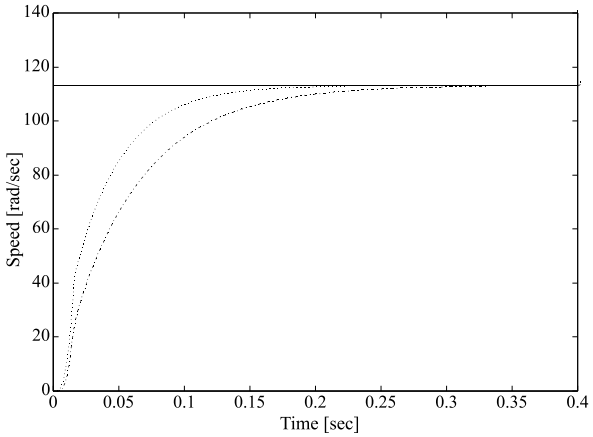

Fig. 21. Speed step responses: the first (dotted) and the second configuration (dashed).

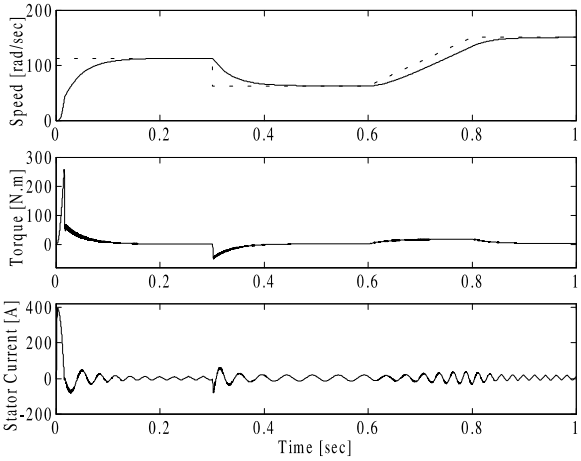

Fig. 22. Speed response following a variable reference.

The drive system is now tested under a variable speed reference and load torque changes simultaneously. The result of Fig. 23 reveals a good control with zero steady state errors and no fluctuations in the drive response. By changing the operating point, the controller is expected to adjust its feedback and integral gains as shown in Fig. 24.

5.4. Comparative Study of FVSC, NIMC and FSFC

The proposed controllers are now compared under the same operating conditions of the drive system. Figure 25 shows the responses under a step change in the speed reference. Under FVSC control, the drive speed response rises slowly with a noticeable overshoot. FSFC exhibits a faster transient response initially but settles down slowly. According to Fig. 25, NIMC leads to shorter rising and settling times. The results demonstrate comparable steady state performance.

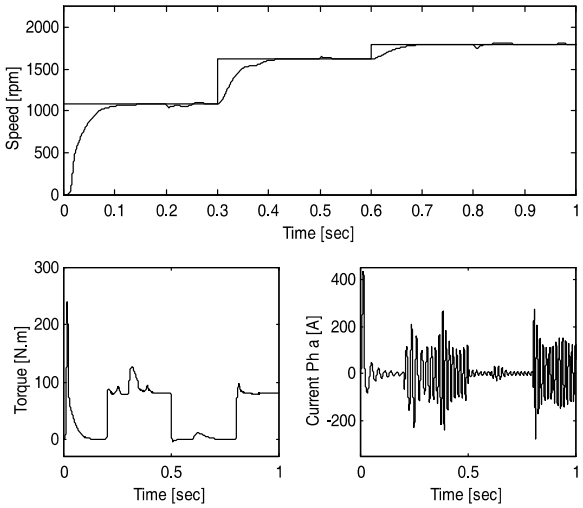

Fig. 23. Speed response under load torque variations.

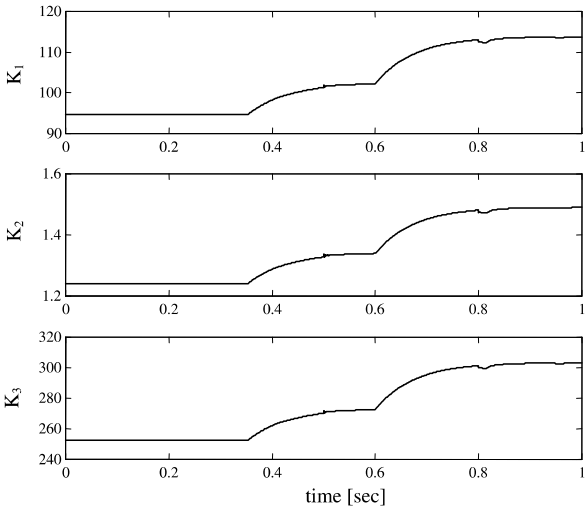

Fig. 24. Controller gains variations.

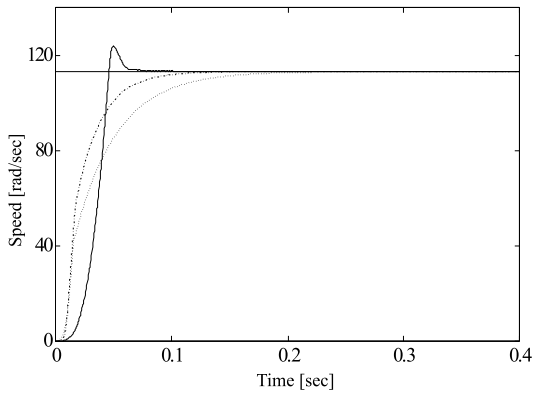

Fig. 25. Drive speed step response: FVSC (solid), FSFC (dotted), and NIMC (dashed).

The quantitative criteria for measuring the performance are chosen as IAE (Integral of the Absolute Error) and ITAE (Integral of Time weigthed Absolute Error):

$$\text{IAE} = \int |e|\,\mathrm{d}t, \quad \text{ITAE} = \int t\,|e|\,\mathrm{d}t. \tag{31}$$

IAE accounts mainly for errors at the beginning of the response and to a lower degree for the steady state deviation. ITAE takes account of the error at the beginning but also emphasises the steady state. The drive system is subjected to a constant step input and the simulation time of 1 sec is taken. The results summarized in Table 3 confirm that NIMC achieves a better transient performance than FSFC and FVSC.

Table 3. Comparative performance with integral criteria.

	IAE	**ITAE**
FVSC	5.9110	0.0059
FSFC	4.2727	0.0021
NIMC	2.9038	0.0014

It is well known that during the normal operation of a drive, induction motor parameters undergo variations due to thermal changes, saturation and other non-linear effects. Among these there is a rotor resistance, which, in turn, causes the rotor time constant to vary sometimes up to 50%. As stated above, this results in performance deterioration of the FOC.

In the next simulation result, the robustness of the three controllers with respect to a variation in the rotor time constant is investigated. This situation is simulated by a linear variation in the rotor resistance such that $R_r = 0.0764(1 + 2.5t)$ corresponding to a variation of 50% in the rotor time constant. Figure 26 illustrates the results of this simulation. The dotted line corresponds to a constant R_r while the solid one is related to a variable R_r. At $t = 0.4$ s, where R_r is twice as large as its nominal value, a second step change in the speed reference is applied. From Fig. 26(a) it can be seen that FVSC is slightly affected while NIMC (Fig. 26(b)) and FSFC (Fig. 26(c)) demonstrate robust performance to R_r variations.

6. Conclusions

This paper presents some design approaches to hybrid control architectures combining conventional control techniques with fuzzy logic and neural networks. Such hybrid structures lead to robust and easily tuned controllers, and are very well suited for systems with uncertain or unknown variations in plant parameters and structure. The induction motor is one of such difficult systems

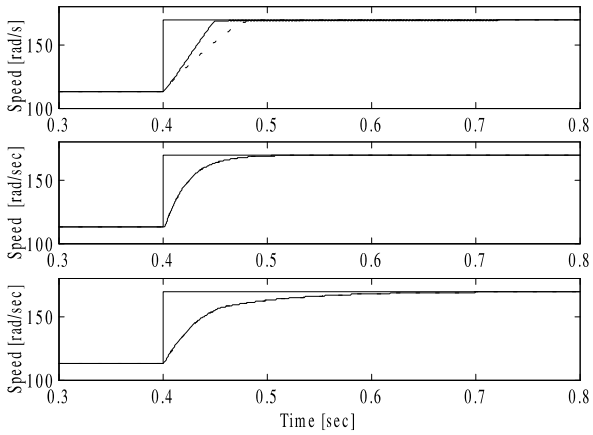

Fig. 26. Performance of (a) FVSC, (b) NIMC and (c) FSFC under variable R_r, R_r = constant (solid) and $R_r = 0.0764(1 + 2.5t)$ (dashed).

and hence it can be considered as a challenging engineering problem for evaluating the performances of the designed controllers.

The performance and robustness of the proposed controllers have been evaluated under a variety of operating conditions of the drive system, and the results demonstrate the effectiveness of these control structures. A comparative study of the control strategies in terms of performance and robustness has been conducted. The performance is maintained under rotor resistance variations, which is known to cause performance deterioration in vector-controlled induction motors.

NIMC and FSFC achieved slightly improved results compared with FVSC, although their synthesis was based on the reduced-order model of the SCIM. The control techniques studied are very suitable for real time implementation due to their simplicity, robustness and ease of tuning.

References

Brdyś M.A. and Kulawski G.J. (1999): *Dynamic neural controllers for induction motor*. — IEEE Trans. Neur. Netw., Vol. 10, No. 2, pp. 340–355.

Cao S.G., Rees N.W. and Feng G. (1999): *Analysis and design of fuzzy control systems using dynamic fuzzy state space models*. — IEEE Trans. Fuzzy Syst., Vol. 7, No. 2, pp. 192–199.

Chan C.C. and Wangs H. (1990): *An effective method for rotor time constant identification for high performance induction motor vector control*. — IEEE Trans. Indust. Electr., Vol. 37, No. 6, pp. 477–482.

Chen C-Li and Chang M-Hui (1998): *Optimal design of fuzzy sliding mode control: A comparative study*. — Fuzzy Sets Syst., Vol. 93, pp. 37–48.

Chin T., Miyashita I. and Koga T. (1996): *Sensorless induction motor drive: An innovative component of advanced motion control*. — Proc. IFAC 13-th World Congress, San-Francisco, USA.

Elloumi M., Al-Hamadi A. and Ben-Brahim L. (1998): *Survey of speed sensorless controls of induction motor drive*. — Proc. IEEE/IECON'98 Conf. Record, Aachen, Germany, pp. 1018–1023.

Hung J.Y., Gao W. and Hung J.C. (1993): *Variable structure control: A survey*. — IEEE Trans. Industr. Electr., Vol. 40, No. 1, pp. 2–21.

Hunt K.J. and Sbarbaro D. (1991): *Neural networks for nonlinear model control*. — IEE Proc., Part D, Vol. 138, pp. 431–438.

Hunt K.J., Sbarbaro D., Zbikowski R. and Gawthrop P.J. (1992): *Neural networks for control systems: A survey*. — Automatica, Vol. 28, pp. 1083–1112.

Kawaji S. and Matsunaga N. (1994): *Fuzzy control of VSS type and its robustness*, In: Fuzzy Control Systems (A. Kandel and G. Langholz, Eds.). — Boca Raton, pp. 226–242.

Kim Y.H., Kim S.S. and Hong I.P. (1998): *Speed sensorless vector control of high speed induction motor using intelligent control algorithm*. — Proc. IEEE/IECON'98 Conf. Record, Aachen, Germany, pp. 888–892.

Kung Y.S., Liaw C.M. and Ouyang M.S. (1995): *Adaptive speed control for induction motor drives using neural networks*. — IEEE Trans. Industr. Electr., Vol. 42, No. 1, pp. 25–32.

Kwan C.M. and Lewis F.L. (2000): *Robust backstepping control of induction motors using neural networks*. — IEEE Trans. Neur. Netw., Vol. 11, No. 5, pp. 1178–1187.

Lee C.C. (1990): *Fuzzy logic in control systems: Fuzzy logic controller – Parts I and II*. — IEEE Trans. Syst. Man Cybern., Vol. 20, No. 2, pp. 404–435.

Mei F., Zhihong M., Yu X. and Nguyen T. (1998): *A robust tracking control scheme for a class of non-linear Systems with fuzzy nominal models*. — Appl. Math. Comp. Sci., Vol. 8, No. 1, pp. 145–158.

Morari M. and E. Zafiriou E. (1989): *Robust Process Control*. — Englewood Cliffs, NJ: Prentice Hall.

Palm R. (1994): *Robust control by fuzzy sliding mode*. — Automatica, Vol. 30, pp. 1429–1437.

Shaw A. and Doyle F. (1997): *Multivariable non-linear control application for a high purity distillation column using a recurrent dynamic neuron model*. — J. Process Contr., Vol. 7, No. 4, pp. 255–268.

Si J. and Zhou G. (1996): *A reduced memory Levenberg-Marquardt algorithm*. — Proc. 13-th IFAC World Congress, San Francisco, USA, pp. 233–236.

Tajima H. (1993): *Speed sensorless field orientation control of induction motor*. — IEEE Trans. Industr. Applic., Vol. 29, No. 1, pp. 175–181.

Trzynadlowski A.M. (1994): *The Field Orientation Principle in Control of Induction Motors*. — Dordrecht: Kluwer.

Umanand L. and Bhat S.R. (1994): *Adaptation of the rotor time constant for variation in rotor resistance of induction motor*. — Proc. IEEE Annual Meeting, Denver, pp. 738–743.

Vas P. (1990): *Vector Control of AC Machines*. — London: Oxford University Press.

Zhen L. and Xu L. (1998): *Sensorless field orientation control of induction machines based on mutual MRAS scheme*. — IEEE Trans. Industr. Electr., Vol. 45, No. 5, pp. 824–830.

List of Symbols and Abbreviations

P_n	nominal power
$T_e,\ T_L$	electromagnetic and load torques
J	rotor inertia
p	pairs of poles
ω	motor speed
$R_s,\ R_r$	stator and rotor resistances
$L_s,\ L_r$	stator and rotor inductance
L_m	mutual inductance
T_r	rotor time constant
$[i^s_{ds}\ \ i^s_{qs}]$	d- and q-axis stator currents
$[i^s_{dr}\ \ i^s_{qr}]$	d- and q-axis rotor currents
$[V^s_{ds}\ \ V^s_{qs}]$	d- and q-axis stator voltages
$[i^{e^*}_{ds}\ \ i^{e^*}_{qs}]$	stator current references
$[\Phi^s_{dr}\ \ \Phi^s_{qr}]$	flux linkages in the stator reference frame
R^i	rule related to the i-th operating point
L	number of operating points
F^i_j	fuzzy sets for the state variables
SCIM	squirrel-cage induction motor
FOC	field orientation control
PID	proportional-integral-derivative
VSC	variable structure controller
VSS	variable structure system
FLC	fuzzy logic controller
NB	negative big
NM	negative medium
NS	negative small
EZ	equal zero
PS	positive small
PM	positive medium
PB	positive big
FVSC	fuzzy variable structure control
IMC	internal model controller
ANN	artificial neural networks
LMA	Levenberg-Marquardt algorithm
MLP	multilayer perceptron
NIMC	neural internal model control
FSFC	fuzzy state feedback control

Appendix A

The SCIM parameters are as follows:

P_n	nominal power	15 kW
R_s	stator resistance	0.1062 Ω
R_r	rotor resistance	0.0764 Ω
L_s	stator inductance	0.01604 H
L_r	rotor inductance	0.01604 H
L_m	mutual inductance	0.01547 H
J	rotor inertia	0.01768 kg.m^2
$2p$	number of pole pairs	4

Appendix B

Starting from the flux equations

$$\Phi^s_s = L_s i^s_s + L_m i^s_r, \quad \Phi^s_r = L_m i^s_s + L_r i^s_r, \tag{B1}$$

the expressions for Φ^s_s and i^s_r can be obtained as

$$\Phi^s_s = \frac{L_m}{L_r}\Phi^s_r + \sigma L_s i^s_s, \quad i^s_r = \frac{1}{L_r}\left(\Phi^s_r - L_m i^s_s\right). \tag{B2}$$

Substitution of (B2) in the drive voltage equations gives

$$V^s_s = R_s i^s_s + s\Phi^s_s, \quad V^s_r = R_r i^s_r + (s - j\omega)\,\Phi^s_r. \tag{B3}$$

Hence

$$s\begin{bmatrix}\Phi^s_{dr}\\ \Phi^s_{qr}\end{bmatrix} = \frac{L_r}{L_m}\left(\begin{bmatrix}V^s_{ds}\\ V^s_{qs}\end{bmatrix} - \begin{bmatrix}R_s + s\sigma L_s & 0\\ 0 & R_s + s\sigma L_s\end{bmatrix}\begin{bmatrix}i^s_{ds}\\ i^s_{qs}\end{bmatrix}\right), \tag{B4}$$

$$s\begin{bmatrix}\Phi^s_{dr}\\ \Phi^s_{qr}\end{bmatrix} = \frac{1}{T_r}\left(L_m\begin{bmatrix}i^s_{ds}\\ i^s_{qs}\end{bmatrix} - \begin{bmatrix}1 & \omega T_r\\ -\omega T_r & 1\end{bmatrix}\begin{bmatrix}\Phi^s_{dr}\\ \Phi^s_{qr}\end{bmatrix}\right). \tag{B5}$$

Equations (B4) and (B5) represent the rotor flux observers and are termed the *voltage model* and the *current model*, respectively. The rotor flux amplitude and phase are

$$\Phi_r = \sqrt{{\Phi^s_{dr}}^2 + {\Phi^s_{qr}}^2} \ \text{ and } \ \theta_r = \tan^{-1}\left(\frac{\Phi^s_{qr}}{\Phi^s_{dr}}\right). \tag{B6}$$

Differentiating (B6) and substituting (B5) leads to the drive speed

$$\omega = \frac{\mathrm{d}\theta_r}{\mathrm{d}t} - \frac{L_m}{T_r \Phi_r^2} \left(i_{qs}^s \Phi_{dr}^s - i_{ds}^s \Phi_{qr}^s \right). \qquad \text{(B7)}$$

In Fig. B1 a block diagram structure of this observer is given

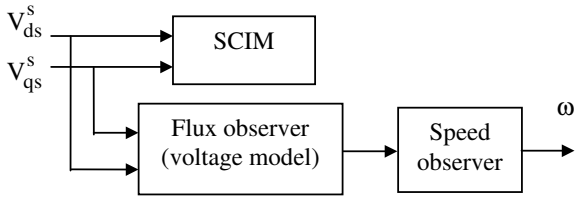

Fig. B1. Block diagram of the speed observer.

Received: 6 June 2001
Revised: 10 September 2001
Re-revised: 18 October 2001